J|A|C|S ARTICLES

Published on Web 11/12/2010

Phosphorus Chemical Shifts in a Nucleic Acid Backbone from Combined Molecular Dynamics and Density Functional Calculations

Jana Přecechtělová,[†] Petr Novák,[†] Markéta L. Munzarová,[†] Martin Kaupp,[‡] and Vladimír Sklenář*,[†]

National Centre for Biomolecular Research, Faculty of Science, Masaryk University, Kotlářská 2, CZ-61137 Brno, Czech Republic, and Institut für Chemie, Technische Universität Berlin, Strasse des 17. Juni 135, D-10623 Berlin, Germany

Received May 31, 2010; E-mail: sklenar@chemi.muni.cz

Abstract: A comprehensive quantum chemical analysis of the influence of backbone torsion angles on ^{31}P chemical shifts in DNAs has been carried out. An extensive DFT study employed snapshots obtained from the molecular dynamics simulation of [d(CGCGAATTCGCG)]$_2$ to construct geometries of a hydrated dimethyl phosphate, which was used as a model for the phosphodiester linkage. Our calculations provided differences of 2.1 ± 0.3 and 1.6 ± 0.3 ppm between the B_I and B_{II} chemical shifts in two B-DNA residues of interest, which is in a very good agreement with the difference of 1.6 ppm inferred from experimental data. A more negative ^{31}P chemical shift for a residue in pure B_I conformation compared to residues in mixed B_I/B_{II} conformation states is provided by DFT, in agreement with the NMR experiment. Statistical analysis of the MD/DFT data revealed a large dispersion of chemical shifts in both B_I and B_{II} regions of DNA structures. δP ranges within 3.5 ± 0.8 ppm in the B_I region and within 4.5 ± 1.5 ppm in the B_{II} region. While the ^{31}P chemical shift becomes more negative with increasing α in B_I-DNA, it has the opposite trend in B_{II}-DNA when both α and ζ increase simultaneously. The ^{31}P chemical shift is dominated by the torsion angles α and ζ, while an implicit treatment of β and ε is sufficient. The presence of an explicit solvent leads to a damping and a 2−3 ppm upfield shift of the torsion angle dependences.

Introduction

Numerous ^{31}P NMR experiments revealed the sensitivity of the ^{31}P chemical shift (δP) to the conformation of the sugar−phosphate backbone in nucleic acids (NA), demonstrating thus the potential of δP to provide valuable structural information.[1] Although spin−spin coupling constants are primarily used to obtain the restraints for torsion angles in biomolecules, such an approach can only be applied to a limited extent in the case of the NA backbone.[2] Six torsion angles define the conformation of the phosphodiester linkage in oligonucleotides (Figure 1).[3] While Karplus equations are available for β, γ, δ, and ε, the torsion angles around P−O bonds cannot be determined since $^3J_{OPOC}$ values are not accessible via experiment.[2,4] The relationships between δP and α/ζ are therefore of particular interest as they could be used to derive restraints unattainable from other sources.

The phosphate groups connecting the sugar moieties undergo a dynamic interconversion between the −gauche/−gauche ($\alpha = -60° \pm 30°$, $\zeta = -60° \pm 30°$) and −gauche/trans ($\alpha = -60° \pm 30°$, $\zeta = 180° \pm 30°$) substates, which are also frequently referred to as B_I- and B_{II}-DNA.[5,6] Since—according to molecular dynamics—the conformational exchange occurs on a nanosecond time scale[7] and since the two substates differ in δP,[1] the experimentally measured values of δ_{iso} represent time averages over both conformations. In order to derive the populations of B_I and B_{II} states, one would have to know the

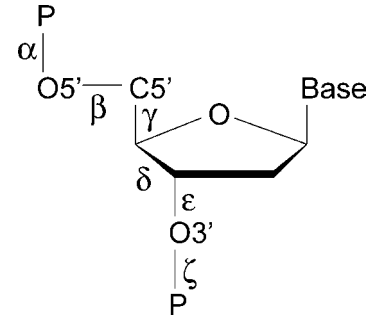

Figure 1. Nucleic acid backbone torsion angles: α (O3′−P−O5′−C5′), β (P−O5′−C5′−C4′), γ (O5′−C5′−C4′−C3′), δ (C5′−C4′−C3′−O3′), ε (C4′−C3′−O3′−P), and ζ (C3′−O3′−P−O5′).

[†] Masaryk University.
[‡] Technische Universität Berlin.

(1) Gorenstein, D. G. *Chem. Rev.* **1994**, *94*, 1315–1338.
(2) Wijmenga, S. S.; van Buuren, B. N. M. *Prog. Nucl. Magn. Reson. Spectrosc.* **1998**, *32*, 287–387.
(3) Saenger, W. *Principles of Nucleic Acid Structure*; Springer-Verlag: New York, 1984.
(4) Sychrovský, V.; Vokáčová, Z.; Šponer, J.; Špacková, N.; Schneider, B. *J. Phys. Chem. B* **2006**, *110*, 22894–22902.
(5) Schneider, B.; Neidle, S.; Berman, H. M. *Biopolymers* **1997**, *42*, 113–124.
(6) Fratini, A.; Kopka, M.; Drew, H.; Dickerson, R. *J. Biol. Chem.* **1982**, *257*, 4686–4707.
(7) Trieb, M.; Rauch, C.; Wellenzohn, B.; Wibowo, F.; Loerting, T.; Liedl, K. R. *J. Phys. Chem. B* **2004**, *108*, 2470–2476.

chemical shift difference $\Delta\delta_{II,I} = \delta_{iso,II} - \delta_{iso,I}$, where $\delta_{iso,I}$ and $\delta_{iso,II}$ are ^{31}P chemical shifts of B_I- and B_{II}-DNA, respectively. The value of $\Delta\delta_{II,I}$ cannot be obtained from experimental measurements of B-DNA duplexes due to the aforementioned $B_I \leftrightarrow B_{II}$ transitions nor from measurements of small compounds due to the absence of rigid −gauche/trans mononucleotides. Therefore, $\Delta\delta_{II,I}$ has to be approximated by the value (1) obtained for other NA types, (2) estimated on the basis of experimental evidence, or (3) obtained from theoretical calculations. Gorenstein used $J_{H3'-P}$ coupling constants, average values of ε, and a plot correlating δP with both ε and $J_{H3'-P}$ to estimate B_I and B_{II} chemical shifts and to determine experimental $\Delta\delta_{II,I}$ to be 1.6 ppm.[1]

Quantum chemical methods are well suited to examine the dependence of δP on backbone torsion angles and thus also to evaluate $\Delta\delta_{II,I}$. The first theoretical account of phosphorus chemical shielding in phosphates was published by Gorenstein and Kar in 1975.[8] In their semiempirical approach, the authors established a linear correlation between CNDO/2 phosphorus electron densities and experimental chemical shifts. The correlation was then used to compute chemical shifts for various conformations of dimethyl phosphate (DMP), resulting in a chemical shielding−torsional angle contour map. Due to the limited structural data used for defining the linear correlation, the map was considered as containing mainly qualitative information. In particular, from the comparison of the ^{31}P chemical shift for an average −gauche/−gauche (gg) state with $\alpha = -60°$, $\zeta = -60°$ (−1 to −2 ppm) and an average −gauche/trans (gt) state with $\alpha = -60°$, $\zeta = 180°$ (−12 ppm), it was concluded that a more negative shift corresponds to more opened (gt) conformations.

In 1979, the first nonempirical calculation was done by Prado et al., who applied ab initio CHF method to study the gauche−gauche and gauche−trans conformations of DMP.[9] The authors concluded that the conformational change between gg and gt forms is accompanied by a bond length and bond angle variation that influences δP more than the change in the torsion angles themselves. Since the approach adopted (calculations on X-ray structures) did not allow a more natural, concerted treatment of torsion angle, bond angle, and bond length changes, only a rough estimate of 4−6 ppm difference between the gg and gt conformations was made. When bond angle and bond length variations were ignored, a gg vs gt difference of 1.5 ppm was obtained, but the value was considered much too small by the authors.

In 1984, using the same method, Giessner-Prettre et al. analyzed δP in terms of PO ester and CO torsion angles.[10] It was concluded that both of these conformational parameters substantially contribute to the value of δP. The largest chemical shielding was obtained when the methyl groups were staggered with respect to the PO bond, whereas the smallest shielding resulted from an eclipsed arrangement. The important influence of the CO torsion angles is further discussed in a 1987 review by Giessner-Prettre and Pullman.[11] A simplified view that only the PO torsion angles dominantly influence the ^{31}P chemical shifts was presented in a 1994 review by Gorenstein.[1] In this work, the 1.5 ppm gg vs gt difference, computed but distrusted by Prado in 1979,[9] was presented as the more reliable of possible B_I/B_{II} differences in δP because of its closeness to the experimental value of 1.6 ppm unknown at the time of the publication by Prado et al. This agreement was probably rather fortuitous, since only the gg conformation subjected to the quantum chemical calculations adopted the structural parameters from X-ray, while the gt conformation was obtained by a simple rotation around one bond without adjusting the bond lengths and angles accordingly.[9]

In the absence of further quantum-chemical studies, there clearly remain several open questions that prevent δP from being used for the structure determination of DNAs. (1) Which of the theoretical B_I/B_{II} differences is relevant to experiment? (2) Are the PO torsion angles in nucleic acids (when coupled with the corresponding change in the local geometry) dominant for ^{31}P chemical shifts? (3) How large is the spread of δP due to variations in β and ε? These and other questions are addressed in the present work.

Apart from quantum-chemical studies, the ^{31}P chemical shift−structure relationships have been studied by analyzing NMR and X-ray data. In particular, linear correlations have been observed between the ^{31}P chemical shifts and three recurrent internucleotide distances as well as between these distances and the difference of ε and ζ.[12] The empirical correlations already proved useful in deriving distance restraints for NMR structure calculations.[13] As such, they represent a crucial step in exploring ^{31}P chemical shielding−structure relationships and offer a view complementary to the work presented here.

We have recently used density functional theory (DFT) to study the influence of both torsion angles and explicit solvent on isotropic ^{31}P chemical shifts in DNAs and RNAs.[14,15] Clusters of DMP with six water molecules were employed to model the backbone phosphate groups and their first solvation shell. NMR calculations were performed with two types of geometry-optimized clusters, differing in the arrangements of the six water molecules around the phosphate anionic oxygens. The values of $\Delta\delta_{II,I}$ obtained for the two static models amounted to 5.9 and 3.8 ppm. This considerably overestimates the 1.6 ppm derived for DNAs by Gorenstein.[1] Moreover, close energies of DMP−water clusters indicated that the system could switch between the two and/or other arrangements of water molecules in solution.

The static approach used previously suffers from a simplified solvent description, an inclusion of both realistic and unrealistic torsion angle combinations, and the lack of backbone dynamics. These limitations of the static model can be overcome by combining quantum chemical calculations with molecular dynamics (MD). The approach has been successfully used to calculate EPR[16−24] as well as NMR parameters.[25] While for NMR of small molecules, ab initio MD could be employed,[26−30]

(8) Gorenstein, D. G.; Kar, D. *Biochem. Biophys. Res. Commun.* **1975**, *65*, 1073–1080.
(9) Prado, F. R.; Giessner-Prettre, C.; Pullman, B.; Daudey, J. P. *J. Am. Chem. Soc.* **1979**, *101*, 1737–1742.
(10) Giessner-Prettre, C.; Pullman, B.; Prado, F. R.; Cheng, D. M.; Iuorno, V.; Ts'o, P. O. P. *Biopolymers* **1984**, *23*, 377–388.
(11) Giessner-Prettre, C.; Pullman, B. *Q. Rev. Biophys.* **1987**, *20*, 113–172.
(12) Heddi, B.; Foloppe, N.; Bouchemal, N.; Hantz, E.; Hartmann, B. *J. Am. Chem. Soc.* **2006**, *128*, 9170–9177.
(13) Abi-Ghanem, J.; Heddi, B.; Foloppe, N.; Hartmann, B. *Nucleic Acids Res.* **2010**, *38*, e18.
(14) Přecechtělová, J.; Munzarová, M. L.; Novák, P.; Sklenář, V. *J. Phys. Chem. B* **2007**, *111*, 2658–2667.
(15) Přecechtělová, J.; Padrta, P.; Munzarová, M. L.; Sklenář, V. *J. Phys. Chem. B* **2008**, *112*, 3470–3478.
(16) Houriez, C.; Ferré, N.; Masella, M.; Siri, D. *J. Chem. Phys.* **2008**, *128*, 244504.
(17) Pavone, M.; Benzi, C.; De Angelis, F.; Barone, V. *Chem. Phys. Lett.* **2004**, *395*, 120–126.
(18) Pavone, M.; Cimino, P.; De Angelis, F.; Barone, V. *J. Am. Chem. Soc.* **2006**, *128*, 4338–4347.

in the case of larger systems such as protein models, classical MD was the method of choice.[31−36]

In this work, we combine MD with static DFT calculations to address the following points. First, we examine the dependence of δP on the backbone torsion angles α and ζ using conformational averaging to select realistic torsion angle combinations. Second, we investigate how the instantaneous solute−solvent interactions present in solution affect the trends in δP due to changes in α and ζ. Third, we use the averaging of chemical shifts over the MD trajectory to determine the difference in δP of B_I and B_{II} conformations. Finally, we compare the results of the MD/DFT study with experiment as well as with the results obtained for static models. Our system of choice is a canonical B-DNA with the sequence [d(CGCGAATTCGCG)]$_2$, the Drew−Dickerson dodecamer (DD), the structure of which has been studied extensively by both X-ray and NMR.[37,38] To the best of our knowledge, this work is the first application of the MD/DFT approach to DNAs.

Methods and Computational Details

MD Simulation. Classical MD simulation of DD has been carried out in explicit solvent using Amber 7.0 program suite,[39] starting from the NMR structure 1NAJ.[37] The system was neutralized using Na^+ ions distributed using the Xleap module of Amber and defined by the force field parm99.[40] The same parameters were used for additional Na^+ and Cl^- ions added to 150 mM concentration. A periodically repeating truncated octahedron water box of size 61 × 61 × 61 Å containing 5501 water molecules has been employed. Constant pressure conditions (1 atm) and constant temperature (300 K) maintained using the Berendsen weak-coupling technique[41] with a time constant of 5.0 ps were used. The simulation utilized particle mesh Ewald summation[42] with a 9 Å cutoff for nonbonding interactions and an integration step of 2 fs. Following a 150-ps system equilibration, we performed a 24.0-ns MD run (consisting of 1-ns parts) with the recently implemented parmbsc0[43] force field. The latter is recommended to avoid a too-frequent presence of artificial α/γ transitions found in the simulations with the older parm99 force field.[44]

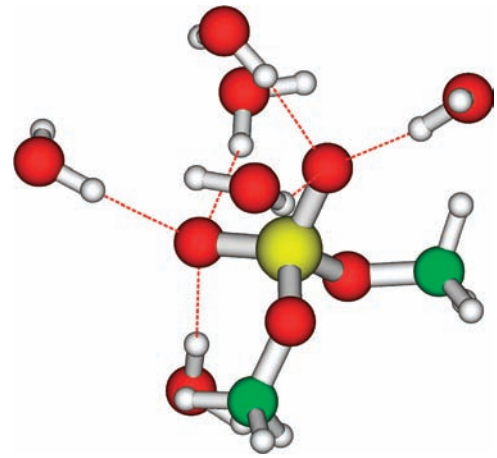

Figure 2. Cluster model composed of dimethyl phosphate and water molecules of the first solvation shell hydrogen-bonded to the anionic phosphate oxygens.

We employ classical MD (instead of the quantum MD) because of the size of the system studied. While classical force fields can suffer from inaccuracies due to the neglect of charge transfer, the parmbsc0 force field employed in our work provides results that are in a very good agreement with experiment in terms of conformation and flexibility.[45] We refer to recent studies covering a broad range of oligomeric sequences of B-DNA (as well as various RNAs, triplex DNA, and Z-DNA)[43] and to a detailed analysis of a microsecond simulation of the DD oligomer.[46]

Molecular Geometries. MD snapshots have been extracted from the entire length of the 24-ns trajectory with a 4-ps time step. Cluster models consisting of DMP and explicit water molecules (Figure 2) were constructed from the G4pA5, C9pG10, and T7pT8 steps of DD, which will from now on be abbreviated as residues G4, C9, and T7, respectively. The reasons for the selection will be given in the Discussion. A total of 6000 geometries were obtained for all residues studied except C9, for which the region between ~16 000 and ~17 400 ps was excluded because of an α/γ switch. The cluster models were cut out from the MD frames, saturating broken bonds with a H-atom bonded to a C-atom with a C−H bond length of 1.09 Å. The clusters included only those water molecules directly hydrogen-bonded to phosphate anionic oxygens. No water molecules hydrogen-bonded to O3′ and O5′ have been considered since X-ray structures revealed that ester oxygens are only responsible for ~15% of all phosphate−water contacts.[47] The following criteria

(19) Brancato, G.; Rega, N.; Barone, V. *J. Am. Chem. Soc.* **2007**, *129*, 15380–15390.
(20) Pauwels, E.; Verstraelen, T.; De Cooman, H.; Van Speybroeck, V.; Waroquier, M. *J. Phys. Chem. B* **2008**, *112*, 7618–7630.
(21) Asher, J. R.; Doltsinis, N. L.; Kaupp, M. *J. Am. Chem. Soc.* **2004**, *126*, 9854–9861.
(22) Asher, J. R.; Doltsinis, N. L.; Kaupp, M. *Magn. Reson. Chem.* **2005**, *43*, S237–S247.
(23) Asher, J. R.; Kaupp, M. *ChemPhysChem* **2007**, *8*, 69–79.
(24) Asher, J. R.; Kaupp, M. *Theor. Chem. Acc.* **2008**, *119*, 477–487.
(25) Searles, D. J.; Huber, H. Molecular Dynamics and NMR Parameter Calculations. In *Calculation of NMR and EPR Parameters: Principles and Applications*; Kaupp, M., Bühl, M., Malkin, V. G., Eds.; Wiley-WCH: Weinheim, 2004; pp 175−189.
(26) Pennanen, T. S.; Vaara, J.; Lantto, P.; Sillanpää, A. J.; Laasonen, K.; Jokisaari, J. *J. Am. Chem. Soc.* **2004**, *126*, 11093–11102.
(27) Pennanen, T. S.; Lantto, P.; Sillanpää, A. J.; Vaara, J. *J. Phys. Chem. A* **2007**, *111*, 182–192.
(28) Ramalho, T. C.; da Cunha, E. F. F.; de Alencastro, R. B. *J. Phys.-Condens. Matter* **2004**, *16*, 6159–6170.
(29) Dračínský, M.; Kaminský, J.; Bouř, P. *J. Phys. Chem. B* **2009**, *113*, 14698–14707.
(30) Dračínský, M.; Bouř, P. *J. Chem. Theory Comput.* **2010**, *6*, 288–299.
(31) Woolf, T. B.; Malkin, V. G.; Malkina, O. L.; Salahub, D. R.; Roux, B. *Chem. Phys. Lett.* **1995**, *239*, 186–194.
(32) Scheurer, C.; Skrynnikov, N. R.; Lienin, S. F.; Straus, S. K.; Brüschweiler, R.; Ernst, R. R. *J. Am. Chem. Soc.* **1999**, *121*, 4242–4251.
(33) Case, D. A.; Scheurer, C.; Brüschweiler, R. *J. Am. Chem. Soc.* **2000**, *122*, 10390–10397.
(34) Markwick, P. R. L.; Sprangers, R.; Sattler, M. *J. Am. Chem. Soc.* **2003**, *125*, 644–645.
(35) Markwick, P. R. L.; Sprangers, R.; Sattler, M. *J. Am. Chem. Soc.* **2003**, *125*, 6337.
(36) Markwick, P. R. L.; Sattler, M. *J. Am. Chem. Soc.* **2004**, *126*, 11424–11425.
(37) Wu, Z.; Delaglio, F.; Tjandra, N.; Zhurkin, V. B.; Bax, A. *J. Biomol. NMR* **2003**, *26*, 297–315.
(38) Drew, H. R.; Wing, R. M.; Takano, T.; Broka, C.; Tanaka, S.; Itakura, K.; Dickerson, R. E. *Proc. Natl. Acad. Sci. U.S.A.* **1981**, *78*, 2179–2183.
(39) Case, D. A.; et al. *AMBER 7*; University of California: San Francisco, 2002.
(40) Cheatham, T., III; Cieplak, P.; Kollman, P. *J. Biomol. Struct. Dyn.* **1999**, *16*, 845–862.
(41) Berendsen, H. J. C.; Postma, J. P. M.; van Gunsteren, W. F.; DiNola, A.; Haak, J. R. *J. Chem. Phys.* **1984**, *81*, 3684–3690.
(42) Darden, T.; York, D.; Pedersen, L. *J. Chem. Phys.* **1993**, *98*, 10089–10092.
(43) Pérez, A.; Marchán, I.; Svozil, D.; Šponer, J.; Cheatham, T. E., III; Laughton, C. A.; Orozco, M. *Biophys. J.* **2007**, *92*, 3817–3829.
(44) Várnai, P.; Djuranovic, D.; Lavery, R.; Hartmann, B. *Nucleic Acids Res.* **2002**, *30*, 5398–5406.
(45) Lavery, R.; et al. *Nucleic Acids Res.* **2010**, *38*, 299–313.
(46) Pérez, A.; Luque, F. J.; Orozco, M. *J. Am. Chem. Soc.* **2007**, *129*, 14739–14745.
(47) Schneider, B.; Patel, K.; Berman, H. M. *Biophys. J.* **1998**, *75*, 2422–2434.

were imposed to determine the presence of a hydrogen bond: $R(PO\cdots H_w) \leq 2.25$ Å and $\angle(PO\cdots H-O_w) \geq 135°$. For a comparison, we have also carried out calculations for DMP stripped of the coordinated water molecules. The geometries of the models extracted from the MD snapshots were used for NMR calculations without performing any structure optimization. Sodium ions were not included in the model. While in principle the effect of counterions on the ^{31}P chemical shift can be large in the case of ions directly coordinated to phosphates,[48] the Na^+ ions only interact with the phosphate group through a water molecule.[49,50] Their expected effect on δP is thus largely indirect[51,52] and is already included in the MD structures.

Chemical Shift Calculations. Chemical shifts for the models constructed from the MD snapshots have been obtained at the DFT level, applying the gradient-corrected BP86 functional[53,54] and locally dense basis sets:[55] IGLO-III basis sets[56] for the phosphorus and oxygen atoms in DMP, and Gaussian-type DZVP orbital basis sets[57] for the methyl groups in the DMP and water molecules. The RI-DFT approximation[58] employed in the wave function calculation part additionally required the use of TZVP and DZVP auxiliary basis sets[59−61] for density fitting. The systematic errors introduced by the use of locally dense basis sets instead of IGLO-III are negligible and generally smaller than the systematic errors in δ_{iso} resulting from the RI approximation, which amount to ~0.5 ppm according to test calculations. The converged Kohn−Sham molecular orbitals have been obtained in Turbomole5.6[62−64] upon imposing the following SCF convergence criteria: 1.10^{-8} au for energy and 1.10^{-7} au for density.

Kohn−Sham orbitals obtained at the computational levels described above were transferred by Turbomole-to-Mag and Gaussian-to-Mag interface routines[65] to the property module MAG of the ReSpect code.[66] Chemical shift calculations in MAG employed sum-over-states density functional perturbation theory with the IGLO choice of the gauge origin (SOS-DFPT-IGLO).[67] Molecular orbitals were localized by the method of Boys,[68] and the LOC1 correction for the energy denominators was used.[67] The chemical shifts were referenced to 85% H_3PO_4 using PH_3 as a secondary standard following the method suggested by van Wüllen,[69]

$$\delta(X, calc) = \sigma(PH_3, calc) - \sigma(X, calc) - 266.1 \qquad (1)$$

where X is the phosphorus atom in the model system of interest and 266.1 ppm is the difference between the absolute experimental chemical shieldings of PH_3 (594.5 ppm) and 85% H_3PO_4 (328.4 ppm) at 300 K.[70] The chemical shielding $\sigma(PH_3,calc)$ is 576.0 ppm at the BP86/IGLO-III level. The use of a secondary standard for ^{31}P has become a frequent method of choice, as the theoretical chemical shielding for 85% H_3PO_4 is hard to obtain.[71]

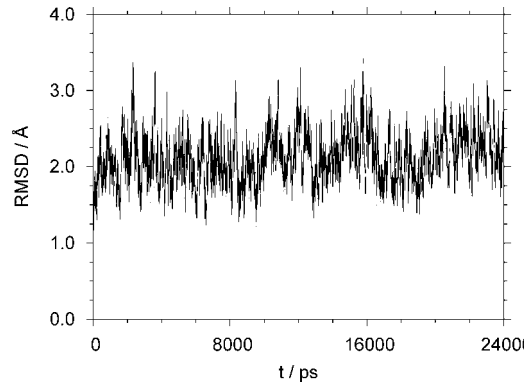

Figure 3. Root-mean-square distance versus starting structure during the MD simulation of $[d(CGCGAATTCGCG)]_2$.

Results and Discussion

1. Molecular Dynamics. A number of MD studies of DD have been published.[72−77,46] In this work, we will discuss those aspects of the MD simulation that are relevant to our objectives. Judging from the root-mean-square distance (rmsd), which fluctuates between ~1.2 and ~3.5 Å (Figure 3), the MD trajectory remains essentially stable for the entire course of 24 ns. The appearance of α/γ switches is rare: the only steps affected are C9pG10 (~16 000−17 400 ps), C1′pG2′ (~11 700−21 900 ps), and A5′pA6′ (~10 500−11 200 ps).

Symmetry and Backbone Substates. A slight asymmetry of the duplex in the simulation is indicated by differences in average P−O torsion angles (Table S1, Supporting Information) and in populations of the B_{II} states between A and B strands of the DNA (Table 1). Considering the length of the trajectory, the distinctions between the strands are not significant. In our calculations, we use the A strand.

Residues G4, C9, and T7 were employed for further analysis for the following reasons. G4 and C9 are well suited for the

(48) Benda, L.; Schneider, B.; Sychrovský, V. Structural ions that are directly coordinated to phosphates may cause non-negligible effects on ^{31}P chemical shielding, to be submitted.
(49) Krasovska, M. V.; Sefcikova, J.; Réblová, K.; Schneider, B.; Walter, N. G.; Šponer, J. *Biophys. J.* **2006**, *91*, 626–638.
(50) Várnai, P.; Zakrzewska, K. *Nucleic Acids Res.* **2004**, *32*, 4269–4280.
(51) Heddi, B.; Foloppe, N.; Hantz, E.; Hartmann, B. *J. Mol. Biol.* **2007**, *368*, 1403–1411.
(52) Wu, Z.; Delaglio, F.; Tjandra, N.; Zhurkin, V. B.; Bax, A. *J. Biomol. NMR* **2003**, *26*, 297–315.
(53) Becke, A. D. *Phys. Rev. A* **1988**, *38*, 3098–3100.
(54) Perdew, J. P. *Phys. Rev. B* **1986**, *33*, 8822–8824.
(55) Chesnut, D. B.; Rusiloski, B. E.; Moore, K. D.; Egolf, D. A. *J. Comput. Chem.* **1993**, *14*, 1364–1375.
(56) Kutzelnigg, W., Fleischer, U., Schindler, M. The IGLO-Method: Ab-initio Calculation and Interpretation of NMR Chemical Shifts and Magnetic Susceptibilities. In *NMR—Basic Principles and Progress*; Springer-Verlag: Berlin/Heidelberg, 1990; Vol. 23, pp 165−262.
(57) Godbout, N.; Salahub, D. R.; Andzelm, J.; Wimmer, E. *Can. J. Chem.-Rev. Can. Chim.* **1992**, *70*, 560–571.
(58) Skylaris, C. K.; Gagliardi, L.; Handy, N. C.; Ioannou, A. G.; Spencer, S.; Willetts, A. *Theochem-J. Mol. Struct.* **2000**, *501*, 229–239.
(59) Eichkorn, K.; Treutler, O.; Öhm, H.; Häser, M.; Ahlrichs, R. *Chem. Phys. Lett.* **1995**, *240*, 283–289.
(60) Eichkorn, K.; Treutler, O.; Öhm, H.; Häser, M.; Ahlrichs, R. *Chem. Phys. Lett.* **1995**, *242*, 652–660.
(61) Eichkorn, K.; Weigend, F.; Treutler, O.; Ahlrichs, R. *Theor. Chem. Acc.* **1997**, *97*, 119–124.
(62) Ahlrichs, R.; Bär, M.; Häser, M.; Horn, H.; Kölmel, C. *Chem. Phys. Lett.* **1989**, *162*, 165–169.
(63) Treutler, O.; Ahlrichs, R. *J. Chem. Phys.* **1995**, *102*, 346–354.
(64) Von Arnim, M.; Ahlrichs, R. *J. Comput. Chem.* **1998**, *19*, 1746–1757.
(65) Kaupp, M.; Reviakine, R.; Malkina, O. L.; Arbuznikov, A.; Schimmelpfennig, B.; Malkin, V. G. *J. Comput. Chem.* **2002**, *23*, 794–803.
(66) Malkin, V. G.; Malkina, O. L.; Reviakine, R.; Arbuznikov, A. V.; Kaupp, M.; Schimmelpfennig, B.; Malkin, I.; Helgaker, T.; Ruud, K. *MAG-ReSpect*, Version 1.1; 2003.
(67) Malkin, V. G.; Malkina, O. L.; Casida, M. E.; Salahub, D. R. *J. Am. Chem. Soc.* **1994**, *116*, 5898–5908.
(68) Edmiston, C.; Ruedenberg, K. *Rev. Mod. Phys.* **1963**, *35*, 457.
(69) van Wüllen, C. *Phys. Chem. Chem. Phys.* **2000**, *2*, 2137–2144.
(70) Jameson, C. J.; De Dios, A.; Jameson, A. K. *Chem. Phys. Lett.* **1990**, *167*, 575–582.
(71) Chesnut, D. B. *J. Phys. Chem. A* **2005**, *109*, 11962–11966.
(72) Ponomarev, S. Y.; Thayer, K. M.; Beveridge, D. L. *Proc. Natl. Acad. Sci. U.S.A.* **2004**, *101*, 14771–14775.
(73) Hamelberg, D.; McFail-Isom, L.; Williams, L. D.; Wilson, W. D. *J. Am. Chem. Soc.* **2000**, *122*, 10513–10520.
(74) Hamelberg, D.; Williams, L. D.; Wilson, W. D. *Nucleic Acids Res.* **2002**, *30*, 3615–3623.
(75) McConnell, K. J.; Beveridge, D. L. *J. Mol. Biol.* **2000**, *304*, 803–820.
(76) Young, M. A.; Ravishanker, G.; Beveridge, D. L. *Biophys. J.* **1997**, *73*, 2313–2336.
(77) Miaskiewicz, K.; Osman, R.; Weinstein, H. *J. Am. Chem. Soc.* **1993**, *115*, 1526–1537.

Table 1. Percentage of the Simulation Time for Which the Backbone of a Given Residue Adopts B_{II} Conformation[a]

	% t_{BII}	
residue	A strand	B strand
G2	14	6
C3	11	12
G4	50	33
A5	14	13
A6	2	0
T7	0	1
T8	2	0
C9	21	8
G10	45	65

[a] Residues located at the end of the DNA strands have been excluded.

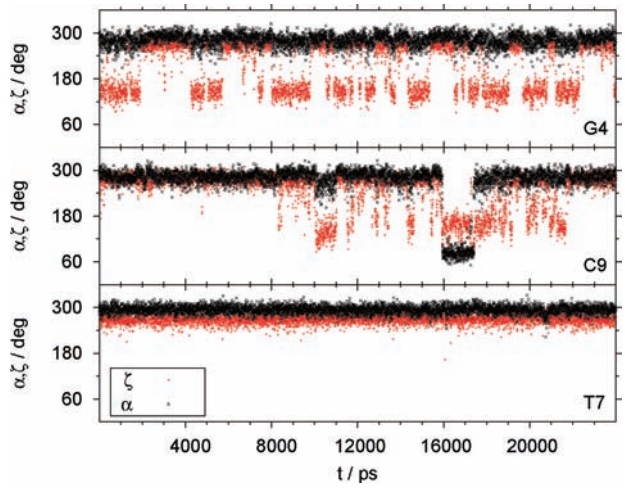

Figure 4. Time dependence of torsion angles α (black) and ζ (red) for residues G4, C9, and T7.

calculation of B_I and B_{II} chemical shifts since they display relatively high percentage of B_{II} conformation (~50% and ~21%, respectively; Table 1). Similar populations were obtained for a much longer, microsecond simulation by Pérez et al.[46] G4 is subject to frequent switches between B_I and B_{II} conformation states during the entire simulation, while the conformation of the C9 phosphate only switches between ~8 and ~22 ns (Figure 4). At the same time, G4 and C9 lie in different parts of the experimental ^{1}H−^{31}P correlation spectrum of DD,[78] with C9 ($\delta_{iso} = -3.9$ ppm) shifted to less negative values of chemical shifts than G4 ($\delta_{iso} = -4.1$ ppm). Residue T7 has been chosen as a pure B_I residue (Figure 4) for a comparison.

Given the B_I/B_{II} conformational transitions and the differences in B_I and B_{II} chemical shifts, the experimental δP values necessarily reflect the percentage occurrence of the two conformations. On the basis of an empirical correlation of experimental δP, sequential interproton distances, and $\varepsilon - \zeta$ differences, Heddi et al. derived an equation relating δP to the percentage of B_{II} by a direct proportionality.[12] An alternative equation was also proposed by Tian et al.[79] The direct proportionality implies that the less negative δP, the higher the percentage of B_{II}, in accord with the early suggestions by

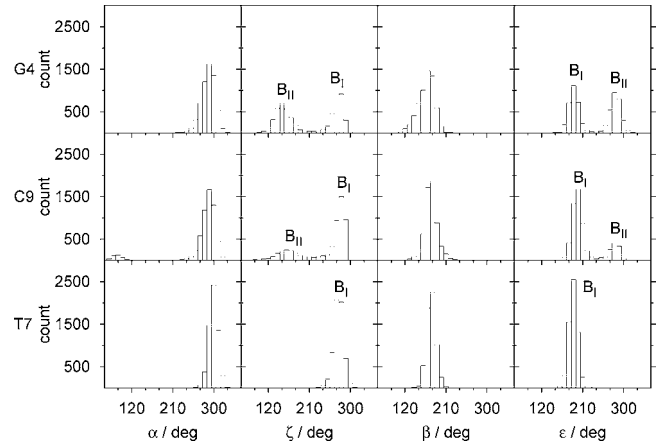

Figure 5. Histograms of torsion angles α, ζ, *β*, and *ε* for junctions G4pA5 (G4), C9pG10 (C9), and T7pT8 (T7) as obtained from the MD simulation.

Gorenstein.[1,80] Using δP of G4 and C9 (cf. above), the equation thus predicts an inverse B_I/B_{II} ratio compared to both our simulation (Table 1) and the microsecond MD simulation by Pérez et al.:[46] a higher percentage of B_{II} for C9 (65%) than for G4 (37%).[79,81] Nevertheless, our results are in accord with those of Schwieters et al., who obtained a higher population of B_{II} for G4 (42%) than for C9 (31%)[82,83] from ensemble refinement against NMR and X-ray data. The disagreement in B_I/B_{II} ratios derived from the linear correlation and from the MD simulation is therefore either due to the limitations of the empirical equation or due to the limitations of the force field, or both.

P−O and C−O Torsion Angles. Histograms of the torsion angles around the P−O bonds are shown in Figure 5, and average torsion angles along with standard deviations of the mean are given in Tables S1 and S2 (Supporting Information). For ζ, a bimodal distribution with a border located at ~210° is found. From now on, the ranges of ζ above and below 210° are denoted as B_I and B_{II} regions, respectively. In order to check whether the MD torsion angles are realistic, we compared values in Tables S1 and S2 for residues G4, C9, and T7 with torsion angles obtained from crystal structures. While our torsion angles for B_I-DNA are within 15° of the mean X-ray values,[84] deviations exceeding 15° have been observed in B_{II}-DNA for α, ζ, and *ε* in G4, α and *β* in C9, and ζ in T7. The most notable difference has been found for ζ and *ε* in G4 (20° and 23°, respectively). Despite the deviations of the average values, our torsion angles still fall within the ranges of X-ray-based histograms for the torsion angles in question.[5] Instead of the mean torsion angle values for B-DNA, it would be more appropriate to compare directly with the crystal structure of DD.[38] Nevertheless, this is hardly possible in the case of B_{II}-DNA since only one junction—G10pC11—adopts the B_{II} conformation in the crystal. Moreover, the junction exhibits a large asymmetry in terms of ζ, which differs by 20° between the A and B strands. The NMR structure 1NAJ[37] from which our simulation started has all residues in B_I conformation. We

(78) Sklenář, V.; Bax, A. *J. Am. Chem. Soc.* **1987**, *109*, 7525–7526.
(79) Tian, Y.; Kayatta, M.; Shultis, K.; Gonzalez, A.; Mueller, L. J.; Hatcher, M. E. *J. Phys. Chem. B* **2009**, *113*, 2596–2603.
(80) Gorenstein, D. G. In *Phosphorus-31 NMR: Principles and Applications*; Gorenstein, D. G., Ed.; Academic Press: Orlando, 1984; pp 7−36.
(81) The percentages of the B_{II} conformation given in brackets were obtained for $T = 299.2$ K.
(82) Schwieters, C. D.; Clore, G. M. *Biochemistry* **2007**, *46*, 1152–1166.
(83) The percentages of the B_{II} conformation given in brackets refer to an ensemble size of $N_e = 8$.
(84) Svozil, D.; Kalina, J.; Omelka, M.; Schneider, B. *Nucleic Acids Res.* **2008**, *36*, 3690–3706.

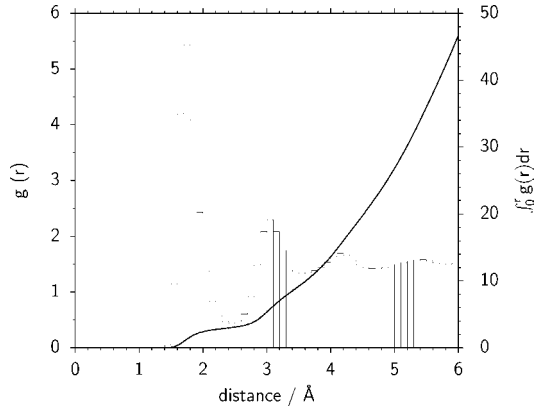

Figure 6. Radial distribution function $g(r)$ for H-bonding distances between O1P/O2P and water protons, and its integral $\int_0^r g(r)\,dr$, representing the number of water molecules found inside a given distance (solid line).

therefore conclude by summarizing that our torsion angles for B_I agree well with the X-ray data, whereas those for B_{II} may be slightly biased by the force field. However, the validation of MD torsion angles against the crystal structure is hampered by the absence of the relevant information for the B_{II} conformation in DD.

Hydration. The solvation of the phosphate group oxygens O1P/O2P is shown in Figure 6 in the form of a radial distribution function (RDF). The first maximum of the RDF indicates that the highest probability of finding a water proton is at the distance of 1.75 Å from either O1P or O2P. The first minimum of the RDF located at 2.45 Å can be considered as a border between the first and second solvation shells. The integral of the RDF indicates the presence of three water molecules per anionic phosphate oxygen, i.e., six water molecules per phosphate, in the first solvation shell of the phosphate group. This is in agreement with early quantum chemical[85] and Monte Carlo simulation[86,87] studies, later confirmed by analyses of DNA crystal structures.[47] The inspection of the residues G4, C9, and T7 reveals that, while 5−6 water molecules occupy the first solvation shell for almost 80% of the simulation time, an occasional occurrence of 3, 4, or 7 water molecules has been observed in the rest of the MD trajectory (Figure S1, Supporting Information). The distribution of H-bond lengths and H-bond angles reveals no significant dependence on the number of water molecules present. Histograms of H-bond lengths and angles integrated over all water occupations are given in Figure S2 of the Supporting Information.

Bond Lengths and Angles. As the snapshots from the simulation serve as a basis for the construction of cluster models that are not optimized subsequently, the quality of the local MD geometry is of a particular concern. In accord with the RDF obtained for the entire duplex (Figure 6), MD hydrogen bond lengths in G4, C9, and T7 range from 1.4 to 2.25 Å, while static structure optimizations of hydrated DMP models provide O1P/O 2P···H_w hydrogen bond lengths of 1.9−2.1 Å. Typical hydrogen bond angles PO···H_w−O_w are 135−175°. A comparison of

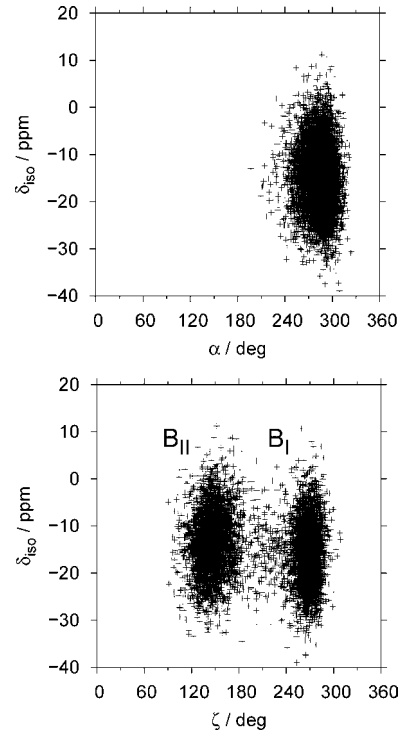

Figure 7. Instantaneous chemical shift values in residue G4 plotted against the torsion angles α (top) and ζ (bottom). The two clusters of data points in the plot for ζ correspond to the B_I and B_{II} conformations.

average bond lengths reveals that MD bond lengths agree within 0.01 Å with bond lengths found in a statistical survey of dinucleoside monophosphates and trinucleoside diphosphates deposited in the Cambridge Structural Database and Nucleic Acid Database.[88] Molecular dynamics also agrees reasonably well with the geometry of DMP optimized with six water molecules at the b3lyp/6-31G(d) level.[14] While MD provides P−O bond lengths shorter by about 0.03−0.05 Å than optimized models, the difference in C−O bond lengths only amounts to 0.01 Å. The MD bond angles also differ by no more than 1° from optimized geometries. The deviations of the MD geometries from their DFT counterparts result in a systematic difference in the absolute chemical shift values. A comparison of δ_{iso} for DMP structures employing molecular parameters obtained from MD in explicit solvent and from structure optimizations of hydrated DMP shows that the phosphorus in the former is by ∼18 ppm more shielded than in the latter. Yet, as we are interested in relative trends rather than in absolute values, we employ no DFT structure optimizations of the cluster models in the combined MD/DFT calculations. Besides the computational feasibility, the approach also provides another advantage. The arrangements of DMP−water clusters as obtained from the simulation of the DNA in explicit solvent best resemble the solution conditions of experimental NMR measurements, while a structure reoptimization may result in fictitious molecular configurations.

2. ^{31}P Chemical Shift Calculations. Dependence on α or ζ: One-Dimensional View. Plotting the ^{31}P chemical shifts obtained for the MD snapshots against α or ζ (Figure 7) results in one or two clusters of data points corresponding to B_I and B_{II} conformation classes. The span of δ_{iso} in the clusters is ∼30

(85) Pullman, B.; Pullman, A.; Berthod, H.; Gresh, N. *Theor. Chim. Acta* **1975**, *40*, 93–111.
(86) Clementi, E. Structure of water and counterions for nucleic acids in solution. In *Structure and Dynamics: Nucleic Acids and Proteins*; Clementi, E., Sarma, R. H., Eds.; Adenine Press: Schenectady, NY, 1983; pp 321−364.
(87) Alagona, G.; Ghio, C.; Kollman, P. A. *J. Am. Chem. Soc.* **1985**, *107*, 2229–2239.
(88) Gelbin, A.; Schneider, B.; Clowney, L.; Hsieh, S. H.; Olson, W. K.; Berman, H. M. *J. Am. Chem. Soc.* **1996**, *118*, 519–529.

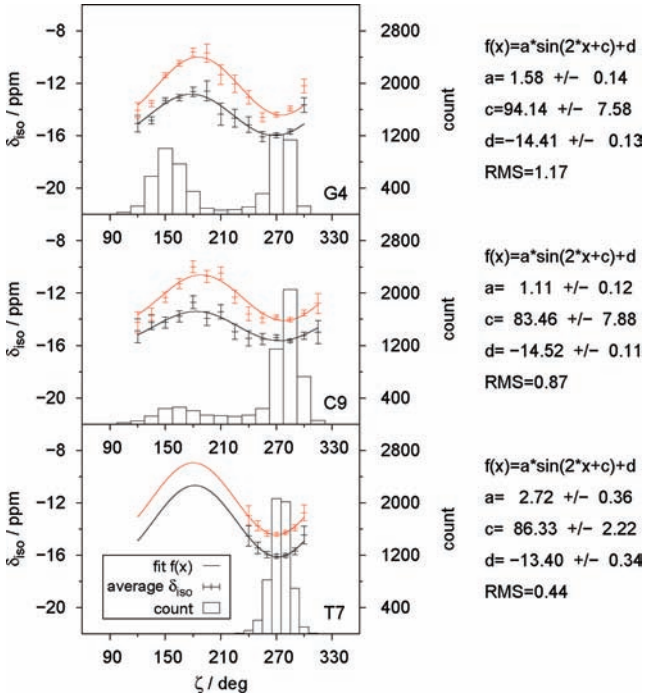

Figure 8. Dependence of the ^{31}P chemical shift on ζ in vacuo (red) and in explicit solvent (black) as obtained from the averaging of chemical shifts in the bins of a histogram.

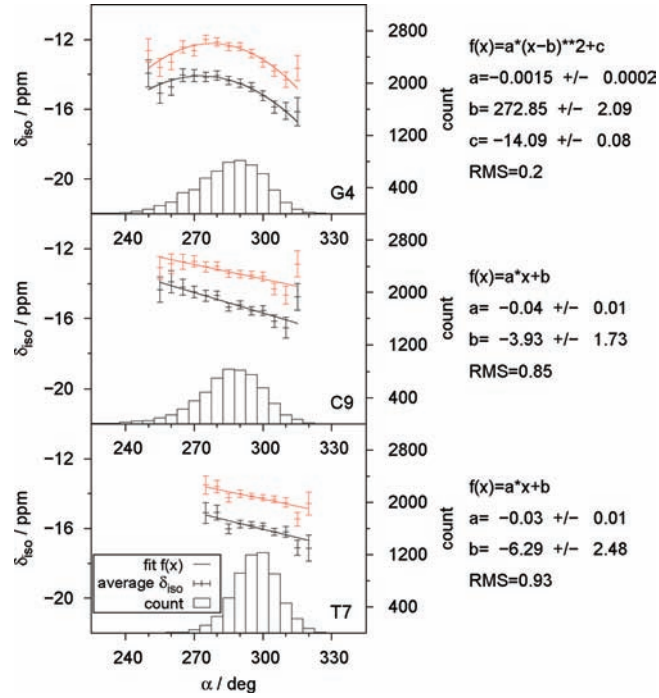

Figure 9. Dependence of the ^{31}P chemical shift on α in vacuo (red) and in explicit solvent (black) as obtained from the averaging of chemical shifts in the bins of a histogram.

ppm for both B_I- and B_{II}-DNA and arises due to the cumulative influence of α, ζ, β, and ε. In order to extract the dependence of δ_{iso} on either α or ζ, we filter out the effects of all torsion angles but the one in question as follows. We divide the ranges of α and ζ into non-overlapping subranges of equal span (15° for G4 and C9, 10° for T7) and average the chemical shifts of those structures for which the P−O torsion angle value falls within the particular subrange. Values falling between α and $\alpha + \Delta\alpha$, where $\Delta\alpha$ is the bin size, are assigned to the bin at $\alpha + \Delta\alpha$ (the same applies to ζ). Due to variable bin populations, the average chemical shifts are obtained with variable precision reflected by the standard deviation of the mean, which we from now on call "the error bar". Only histogram bins with more than 50 data points are considered. The average δ_{iso} values along with the error bars are then plotted against α/ζ and used for a subsequent fitting. The procedure is carried out for chemical shifts obtained in explicit solvent as well as *in vacuo*.

A torsion angle dependence of any property is expressible as an oscillating function with a period of 2π and can always be decomposed into a Fourier series as a sum of sines and/or cosines. In our case, the derivation of the functional dependence is restricted only to populated regions. Figure 8 shows that, within the range of ζ for G4 and C9, the dependences of the chemical shifts can be well approximated by $f(\zeta) = \sin(2\zeta)$, with phase shifts ranging between −35° and −45°. The maxima and minima of the $\sin(2\zeta)$ functions lie at $\zeta = 180°$ and $\zeta = 270°$, respectively, and the difference between them is larger for G4 than for C9 (3 ppm vs 2 ppm in explicit solvent). The distinct amplitudes result from differences in average α, β, and ε. The B_{II}-maximum of the histogram does not coincide with the maximum of the sine function. This indicates that the values of ζ leading to a maximum chemical shift are not those most frequently populated in the MD. The averaging applied as described above does reveal the chemical shift trends due to one desired torsion angle with the effects of the other torsion angles averaged and reflected in corresponding error bars. A connection between the results of the MD/DFT and a static approach, given in the Supporting Information, can provide an insight into the extent of these average effects.

The averaged dependence on α is slightly different for G4 than for C9 and T7 (Figure 9). A quadratic function fits the average values of δ_{iso} between 250° and 315° in G4 with the maximum of the chemical shift dependence being placed around $\alpha = 275°$. In contrast, the ^{31}P chemical shift decreases linearly with an increasing α in the case of C9 and T7. The different trends are due to the adjacent C−O torsion angle that modulates the dependence (cf. Supporting Information). The effect of the adjacent torsion angles is also responsible for the fact that the dependence of the ^{31}P chemical shift on α is different from that on ζ in the corresponding range of angles.

Dependence on α and ζ: Two-dimensional View. Simultaneous effects of α and ζ torsion angles have been studied by creating 2D plots in analogy to Figures 8 and 9. The ranges of the torsion angles were divided into non-overlapping subranges with 10° span. Values of δP falling between α and $\alpha + 10°$ and at the same time between ζ and $\zeta + 10°$ have been assigned to the square-bin at $\alpha + 5°$, $\zeta + 5°$. Averages of δP were then calculated along with the error bars for each bin with no less than 50 data points. This procedure has been carried out for G4, T7, and C9 data separately, as well as for a superposition of G4, T7, and C9 data. The average chemical shifts are shown graphically in Figure 10, while the error bars are listed in the Supporting Information. We note that B_I region for C9 is represented by one square-bin within the 2D representation and by seven bins in the 1D representation. The reason is that spreading-out the sparse B_I data from one to two dimensions decreases populations of most bins below 50. In the joint map (Figure 10d), the covered range is broader than just a superposition of Figure 10a−c, since for many square-bins joining the data increased the populations over 50.

The colored regions plotted in Figure 10 reflect the space of α, ζ combinations most abundant in the MD simulation. We

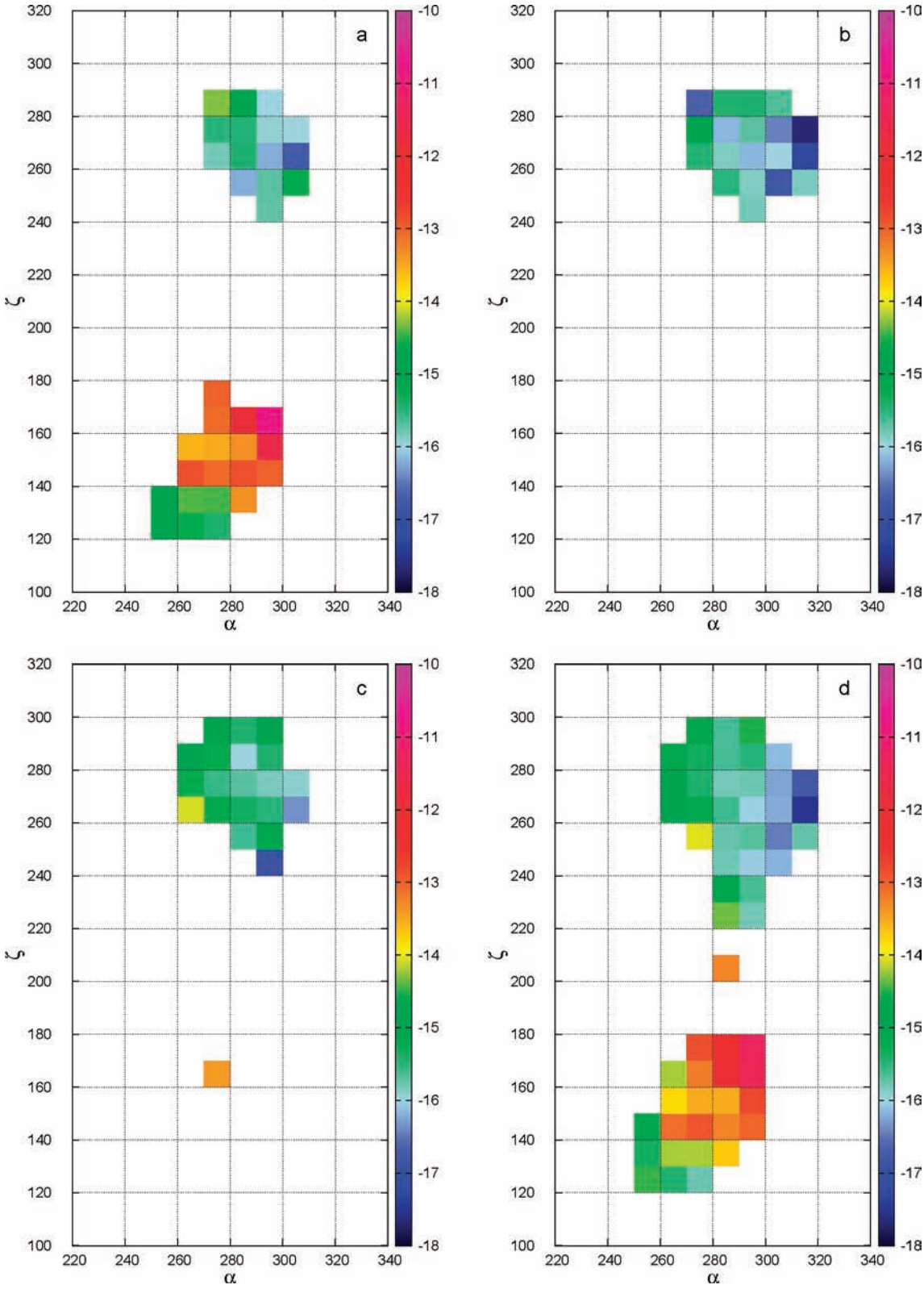

Figure 10. Dependence of δP on α and ζ for residues G4 (a), T7 (b), and C9 (c) and for data summarized over all of G4, T7, and C9 (d).

suppose that the corresponding conformations are likely to be found in real systems, either as X-ray solid-state structures or as average solution structures. Indeed, α, ζ combinations represented in Figure 10 form a subset of α, ζ combinations reported in scattergrams of torsion angles observed in X-ray structures of DNAs.[5,84]

Results in Figure 10 must be understood in the framework of their statistical meaning: two average values are statistically different if their error bars do not overlap. As expected, most information is contained in the superimposed data in Figure 10d that not only cover most of the torsional space but also have a moderate average error bar of 0.54 (ppm), similar to 0.48 for

Table 2. Isotropic Chemical Shifts Obtained by Averaging over the Molecular Dynamics Trajectory[a]

residue	δ_{iso} /ppm	$\delta_{iso,I}$ /ppm	$\delta_{iso,II}$ /ppm	$\Delta\delta_{II,I}$ /ppm
G4	-14.6 ± 0.1	-15.7 ± 0.2	-13.6 ± 0.2	2.1 ± 0.3
C9	-15.1 ± 0.1	-15.5 ± 0.1	-13.8 ± 0.3	1.6 ± 0.3
T7	-15.9 ± 0.1	-15.9 ± 0.1		

[a] The total average and the subaverages for B_I and B_{II} conformation states are given. The standard deviations of the mean given in the table were calculated employing the statistical inefficiency of the simulation (cf. Supporting Information).

T7, and smaller than 0.61 for both G4 and C9. Comparing the color distributions, data for G4, T7, and C9 are similar in that the most negative chemical shifts are obtained for high values of α. However, some of the T7 data are shifted toward more negative values (as found also in the 1D fits, compare with Figure 9). This systematic shift can be a reflection of a change in β and/or ε distribution, which is narrower for T7 than for G4 and C9 (Figure 5). We can thus trace again the perspective of dominating α, ζ and modulating β, ε.

Figure 10 (along with the average δP and the error bars in the Supporting Information) reveals that the least negative chemical shift predicted by our calculations is -11.3 ± 0.9 ppm, and it is obtained for B_{II} structures with combinations of the highest α with the highest ζ (α between 290° and 300°, ζ between 170° and 180°). Starting from this δP value, the chemical shift in the B_{II} region of Figure 10d decreases approximately along the diagonal to -15.8 ± 0.8 ppm. In contrast, the least negative B_I value of δP is -14.0 ± 0.7 ppm for low α (270−280°) and moderate ζ (250−260°) combinations. δP in the B_I region then decreases with increasing α, leading to the most negative chemical shift of -17.5 ± 0.5 ppm for B_I structures with high α (310−320°) and moderate ζ (260−270°). We thus obtain the range of 3.5 ± 0.8 ppm in the B_I region and the range of 4.5 ± 1.5 ppm in the B_{II} region, and an overall range of 6.2 ± 1.0 ppm in the $B_I + B_{II}$ region.

Dependence on β and ε. The effect of β and ε on the ^{31}P chemical shift determined for a 360° rotation around a C−O bond is large (up to ∼3 ppm), yet smaller than that of α and ζ (∼14 ppm, cf. Figure S3 in the Supporting Information). This is in a qualitative agreement with the early results by Giessner-Prettre et al.[10] In contrast to the free rotation, the torsion angles in the MD simulation are confined to boundaries inherent to the flexibility of the B-DNA. In such a case, the effect of β and ε within the averaging approach is less than or equal to the error bar for a given square bin, since the error bar accounts for the variations of δP introduced by (1) all possible changes in β and ε, (2) bin-size changes in α and ζ, and (3) other numerical noise. The error bars for the map in Figure 10d decrease with increasing bin populations, ranging from 0.9 (bin populations close to 50) through 0.5 (populations around 200) to 0.2 (populations higher than 1000, numerical noise minimized). Therefore, the error bar for highly populated bins (0.2 ppm) is close to the average β, ε effect for a bin of 10° width, which is a small number compared to the ∼6 ppm range of δP due to variations in α and ζ. This suggests that an explicit treatment of α and ζ is essential, while β and ε can be accounted for implicitly through the "correct choice" of their values for given α and ζ.

Average Chemical Shifts for the Studied Residues. The averaging over the MD trajectory leads to isotropic chemical shifts of −14.6, −15.1, and −15.9 ppm for residues G4, C9, and T7, respectively (Table 2). The corresponding experimental values are −4.1, −3.9, and −4.4 ppm.[78] Our MD/DFT model thus correctly predicts that T7 is most shielded out of the three residues. However, the theoretical position of G4 with respect to C9 is opposite to the experimental one. (Weighted averages of B_I and B_{II} chemical shifts indicate that the same result would also be obtained for the B strand.) We expect that a slightly larger cluster model and/or a longer MD simulation might help to reproduce the relative experimental chemical shifts of G4 and C9. Considering the extremely narrow span of experimental chemical shifts and the complexity of the system, already the agreement found for the relative position of T7 should be considered as a great success of the model used in our study.

Chemical Shift Difference between B_I and B_{II} States. Since chemical shifts can be averaged separately for each of the two conformation substates, we can evaluate the chemical shift difference $\Delta\delta_{II,I}$. In order to distinguish between B_I- and B_{II}-DNA, we use the border between the peaks in the histogram for ζ (Figure 5) to define structures with $\zeta > 210°$ as B_I state and structures with $\zeta \leq 210°$ as B_{II} state. The obtained $\Delta\delta_{II,I}$ amounts to 2.1 ± 0.3 and 1.6 ± 0.3 ppm for G4 and C9 (Table 2), respectively. The distinct values found for the residues are in accord with the different amplitudes of the sine dependence of the chemical shift on ζ (Figure 8). However, it is important to note that $\Delta\delta_{II,I}$ is not simply equivalent to the difference between the minimum and maximum of the sine function. The value of $\Delta\delta_{II,I}$ represents the difference between the chemical shifts obtained as averages over the entire B_I and B_{II} regions of the histogram for ζ. In contrast, the (double) amplitude of the sinusoid is given by chemical shifts averaged over geometries with ζ falling within 15-deg ranges placed around $\zeta = 180°$ and $\zeta = 270°$. In our previous paper,[14] DFT chemical shift calculations employing clusters of DMP with six water molecules in two distinct arrangements around the phosphate oxygens provided $\Delta\delta_{II,I} = 5.9$ and 3.8 ppm. Comparing these values to the 1.6 ppm difference found by Gorenstein[1] shows that, while static calculations overestimate $\Delta\delta_{II,I}$, combining DFT with MD greatly improves the agreement.

Conclusions

The present study has shed light from various viewpoints on the ^{31}P chemical shifts in a B-DNA backbone, using [d(CGCGAATTCGCG)]$_2$ as the model system. The first question addressed was that of the quantitative accuracy of δP obtainable by the MD/DFT approach. Our calculations provided differences of 2.1 ± 0.3 and 1.6 ± 0.3 ppm between the B_I and B_{II} chemical shifts in two B-DNA residues of interest, which is in a very good agreement with the difference of 1.6 ppm inferred from experimental data. The MD/DFT approach thus brings a considerable improvement over the static model approaches reported so far.

The analysis of the MD/DFT data resulted in a much more refined picture of δP vs structure than available from previous experimental and theoretical studies. Importantly, it revealed a large dispersion of chemical shifts in both B_I and B_{II} conformations of our model. Supposing that the conformations significantly populated in the classical MD simulation are likely to be found in real structures, a whole range of B_I and B_{II} chemical shift values is to be expected in experiment. In particular, δP varies within 3.5 ± 0.8 ppm in the B_I region and within 4.5 ± 1.5 ppm in the B_{II} region, depending on the α, ζ combination. Medium values of the ^{31}P chemical shift are obtained for all B_I structures with $\alpha \leq 280°$ and all B_{II} structures with $\alpha \leq 280°$ and $\zeta \leq 140°$. B_I chemical shifts become more negative with

increasing α, while B_{II} chemical shifts become less negative with increasing α and ζ.

Our results indicate that the α, ζ-based interpretation of ^{31}P chemical shifts in a DNA backbone, disputed in the literature, is indeed possible. An implicit treatment of *β* and *ε* is sufficient. However, the discussion of *δ*P should definitely not be oversimplified to a pure B_I/B_{II} ratio perspective that completely omits the important dependence on the particular α and ζ combination, which characterizes the opening of the backbone.

Looking at the α and ζ angles individually, well-defined (sinusoidal and polynomial) dependences have been established. These dependences are modulated by the adjacent C−O torsion angles *β* and *ε*. The presence of explicit solvent leads to a damping and an upfield shift of the torsion angle dependences by 2−3 ppm with respect to their gas-phase counterparts.

Acknowledgment. The authors thank Juha Vaara (University of Oulu), Roman Martoňák (Comenius University Bratislava), Jiří Šponer (Academy of Sciences of the Czech Republic), Petr Kulhánek, Pavel Kadeřávek, and Dominik Munzar (all Masaryk University) for helpful discussions. This work was supported by the Grants MSM0021622413 to M.M. and LC06030 to V.S. from the Ministry of Education, Youth and Sports of the Czech Republic, and by the Grant No. IAA500040903 from the Grant Agency of the Academy of Sciences of the Czech Republic to J.P. Deutscher Akademischer Austausch Dienst (DAAD) is acknowledged for the scholarship awarded to J.P. for her research stay at the University of Würzburg, Germany. The access to the MetaCentrum supercomputing facilities provided under the research intent MSM6383917201 is highly appreciated.

Supporting Information Available: Average P−O and C−O torsion angles as obtained from the MD simulation; plot of H-bonding configurations at anionic phosphate oxygens O1P and O2P; histograms of H-bond lengths and angles for the water molecules hydrogen-bonded to O1P and O2P; comparison of ^{31}P chemical shift trends obtained from the MD/DFT and a static approach; further discussion of solvent effects; calculation of statistical errors; average ^{31}P chemical shifts (and the standard deviations of the mean) for α, ζ combinations used in Figure 10; complete ref 39. This material is available free of charge via the Internet at http://pubs.acs.org. The structures employed for chemical shift calculations are available upon request from the authors.

JA104564G